Order-controlled closed-loop focal beams and resolution comparison of primary and multiple reflections for seismic acquisition geometries

Wei, Wei; Blacquière, Gerrit

DOI
10.1111/1365-2478.13043

Publication date
2021

Document Version
Accepted author manuscript

Published in
Geophysical Prospecting

ORDER-CONTROLLED CLOSED-LOOP FOCAL BEAMS AND RESOLUTION COMPARISON OF PRIMARY AND MULTIPLE REFLECTIONS FOR SEISMIC ACQUISITION GEOMETRIES

Wei Wei[1,2*], Gerrit Blacquière[3]

[1] *Key Laboratory of Petroleum Resource Research, Chinese Academy of Sciences, Institute of Geology and Geophysics, Beijing, China.*

[2] *Innovation Academy for Earth Science, Chinese Academy of Sciences, Beijing, China.*

[3] *Delft University of Technology, Delphi Consortium, Delft, The Netherlands.*

E-mail: caswei@gmail.com (W. Wei), G.Blacquiere@tudelft.nl (G. Blacquière)

Abstract

Focal beam analysis has built a bridge between the acquisition parameters on the surface and the image quality of underground targets. However, as a practical matter, it is still difficult to answer how to choose a proper acquisition geometry according to the complexity of medium, especially considering the contradictory effects of multiple reflections on spatial resolution as they can be considered to be either potential signal or additional noise, depending on the envisioned imaging technology. We introduce an order-controlled, closed-loop focal beam method in which the migration operator and the resolution function can be analyzed in the process of the closed-loop migration with full control over the order of the surface and internal multiples considered. This method highlights the effects of primary and different-order multiple wavefields on the imaging resolution for different acquisition geometries and various overburden strata. We apply the method to analyze the predicted resolution of seismic acquisition geometries considering multiples as either noise or signal.

Results show, in the acquisition geometry design, that when the primaries cannot provide a complete spatial illumination for the subsurface target, e.g., because of the limited-aperture acquisition geometries or the complicated overburden, we should use the closed-loop focal beam analysis to assess the contradictory effects of multiples as both signal and noise, in which the maximum order of multiples ought to be chosen according to the core aim of the acquisition analysis. We can apply the second-order closed-loop focal beam analysis to quantify the effects of acquisition geometries on multiple-wave suppression, and can also perform the high-order closed-loop focal beam analysis to quantify the effects of acquisition geometries on high-resolution imaging (migration). This method can also be used to choose the optimal order of multiples in the closed-loop migration.

Keywords: Focal beam, Seismic acquisition geometries, resolution, multiples

Introduction

Seismic imaging results often suffer from lack of resolution and signal-to-noise ratio caused by limited-aperture and under-sampled acquisition geometries, which need to be assessed for their performance prior to acquisition, especially for irrecoverable shadow zones of seismic illumination in complex media. Conventional acquisition geometry analysis is usually based on common midpoint (CMP) analysis for horizontally-layered media and the common reflection point (CRP) analysis for complex media, in which acquisition schemes are judged by such properties as fold, offset and azimuth distributions in target bins; see Cordsen et al. (2000) and Vermeer (2012) for details. To measure quantitatively image resolution of acquisition geometries, many approaches have been developed since the early 2000s, e.g., spatial resolution analysis (Vermeer, 1999; Gibson and Tzimeas, 2002; Huang and Schuster, 2014; Schuster et al., 2017) based on the theory of Beylkin (1985), illumination analysis (Wu and Chen, 2006; Xie et al., 2006; Cao and Wu, 2009; Yan and Xie, 2016) based on point spread functions (PSFs) and full sequences of modeling and migration (Jurich et al., 2003; Regone 2006). A more efficient way is the focal beam analysis (Berkhout et al., 2001), which assesses the detector and source sampling separately based on common-focus-point migration (Berkhout, 1997). The focal beam analysis can be applied for both homogeneous media (Volker et al., 2001) and heterogeneous media (Van Veldhuizen et al., 2008; Wei et al., 2012, 2014; Ishiyama et al., 2016). Most of these studies have only considered primary reflections and ignored the effects of multiple reflections in the migration result.

As a physical response of medium discontinuity, multiple reflections propagate along travel paths that differ from the paths of primary reflections and may therefore illuminate

different parts of the subsurface. This potentially leads to improve seismic imaging. Historically, multiple reflections used to be suppressed as noise, but they are now increasingly accepted as signals to provide independent illumination (Berkhout, 2012). Surface multiples can be brought into the imaging by open-loop migration, in which all orders of surface multiples are injected back into the subsurface as primaries to obtain the final image with no iterations (e.g., Verschuur and Berkhout, 1994; Liu et al., 2011; Tu and Herrmann, 2015; Lu et al., 2015). However, in open-loop migration, only parts of the multiples can be focused correctly, while the defocused parts of the multiples manifest as crosstalk noise. This problem will become even more challenging when internal multiples are involved as well. To handle all multiples, closed-loop migration has been proposed by Berkhout (2014), which uses an iterative process of full-wavefield modeling and migration to reconstruct the observed data from the estimated reflectivity and velocity field, as does least-squares migration (Nemeth et al., 1990) in the case of primary-wave reflections. Compared with open-loop migration, closed-loop migration not only balances amplitudes and reduces crosstalk noise, but it also has the flexibility to migrate the full-wavefield seismic data with full control over the order of surface and internal multiples taken into consideration. Based on this, Kumar et al. (2015) extended the focal beam theory to incorporate the illumination of the surface by multiples and then discussed the enhanced illuminating effects of multiples on filling coverage holes (Kumar et al., 2016). However, as a practical matter, it is still difficult to design proper acquisition geometries in the case of complex media, especially considering the contradictory effects of multiples being considered as either potential signal or additional noise depending on the imaging technology used.

For this reason, we extend the full-wavefield focal beams (Kumar et al., 2015, 2016) to an order-controlled closed-loop focal beam method, which provides the flexibility to analyze migration operators and resolution functions with the order-controlled surface and internal multiples in the process of iterative inversion-based migration. In the frameworks of both open-loop and closed-loop focal beams, we compare the temporal and spatial resolution of primary and different-order multiple reflections in simple-layered and complex-structured velocity models. We then investigate the effects of multiple wavefields of different order on the imaging quality for different acquisition geometries and different overburden strata, e.g. a narrow observation aperture, an acquisition obstacle area, a high-velocity overburden, and a complex salt dome. Based on the resulting focal operators and beams, we also discuss the question of how to choose the optimal order of multiples in both focal beam analysis and full-wavefield migration.

Recursive full-wavefield modeling

A seismic reflection data set $\mathbf{P}^{-}(z_d, z_s)$, composed of primaries and multiples (Figure 1), can be formulated using the matrix notation (Berkhout, 1982). For each monochromatic component in the spatial frequency domain the formulation is:

$$\mathbf{P}^{-}(z_d, z_s) = \mathbf{D}^{-}(z_d) \sum_{m=1}^{M} [\mathbf{W}^{-}(z_d, z_t)\mathbf{R}^{\cup}(z_m)\mathbf{G}^{+}(z_t, z_s)]\, \mathbf{S}^{+}(z_s), \tag{1}$$

here,

- superscripts $-$ and $+$ refer to up- and down-going propagations,
- superscripts $\cup$ and $\cap$ refer to down-up and up-down reflections,
- z_d and z_s are the detector and source depths, z_m are the m^{th} $(1 \le m \le M)$ target depth where the waves are reflected,

- $\mathbf{D}^{-}(z_d)$ and $\mathbf{S}^{+}(z_s)$ are the detector and source matrices,
- $\mathbf{R}^{\cup}(z_m)$ is the down-up reflectivity matrix,
- $\mathbf{W}^{-}(z_d, z_m)$ is the detector-side primary-wave upgoing propagation matrix from depth z_m to z_d,
- $\mathbf{G}^{+}(z_m, z_s)$ is the source-side full-wavefield propagation matrix from depth z_s to z_m.

[Figure 1]

The matrix $\mathbf{W}^{-}(z_d, z_m)$ describes primary-wave upgoing propagation at the detector side, and the matrix $\mathbf{G}^{+}(z_m, z_s)$ describes full-wavefield propagation at the source side, including primaries, and surface as well as internal multiples. The full-wavefield propagator $\mathbf{G}^{+}(z_m, z_s)$ is the nonlinear combination of one-way propagation matrices (Thorbecke et al., 2004) and angle-dependent reflectivity matrices (De Bruin et al., 1990), which can be solved in a recursive manner (Davydenko and Verschuur, 2016, 2018). The full-wavefield propagator $\mathbf{G}^{+}(z_m, z_s)$ can be divided into two parts: the primary-wave operator $\mathbf{W}^{+}(z_m, z_s)$ and the multiple-wave operator $\mathbf{M}^{+}(z_m, z_s)$, which can be further decomposed into different orders of multiples based on the number of reflections,

$$\begin{aligned}\mathbf{G}^{+}(z_m, z_s) &= \mathbf{W}^{+}(z_m, z_s) + \mathbf{M}^{+}(z_m, z_s) \\ &= \mathbf{W}^{+}(z_m, z_s) + \mathbf{M}_1^{+}(z_m, z_s) + \mathbf{M}_2^{+}(z_m, z_s) + \cdots,\end{aligned} \tag{2}$$

Equations (1) and (2) are known as recursive full-wavefield modeling (Berkhout, 2012), also called FWMod, which has been used in both full-wavefield modeling and migration (Davydenko and Verschuur, 2016, 2018). Using the FWMod method, we can realize an

efficient 3D wavefield modeling, while having full control over the order of multiple scattering modeled, which is fundamental to the follow-up focal beam analysis.

To illustrate FWMod, we first give an example of the 3D layered velocity model shown in Figure 2a. As part of the computation of a focal beam (Berkhout, et al., 2001), we model a detector-side grid-point response by placing a source at the target point located at (x, y, z) = (3, 3, 1) km. The source emits a Ricker wavelet with a peak frequency of 20 Hz, which will be used in all following examples. The detectors are located at the surface. The modeled wavefields are shown in Figures 2b-d for the first, second and third iteration. The first iteration produces the direct wavefield only, which represents the detector-side primary-wave propagation $\mathbf{W}^{-}(z_d, z_m)$. In subsequent iterations, with higher-order multiples being involved, $\mathbf{M}_1^{-}(z_d, z_m)$, $\mathbf{M}_2^{-}(z_d, z_m)$, etc., are produced, such that gradually the detector-side full-wavefield propagation $\mathbf{G}^{-}(z_d, z_m)$ is obtained. The next example uses a cropped version of the 3D SEG/EAGE salt dome velocity model shown in Figure 3a. We set the target position at (3, 3, 1) km just beneath the salt dome. Using the same source and detector configuration as in the previous example, the resulting detector-side grid-point responses shown in Figures 3b-d indicate that FWMod can simulate the primary and multiple wavefields in a complex medium, making it suitable for computing focal beams. Note that the source-side response can be modeled in the same way as the detector-side response based on the reciprocity theory (e.g. Wapenaar, 1998). These examples clarify the FWMod is flexible and suitable for the subsequent focal beam analysis.

[Figure 2]

[Figure 3]

Open-loop focal beams based on linear migration

Based on the focal beam theory (Berkhout et al., 2001), we apply double focusing at both detector and source sides of a unit angle-independent point diffractor at a target point located at (x_j, y_j, z_m), followed by the imaging principle. The point diffractor is described by matrix $\delta_j \mathbf{R}^{\cup}(z_m)$, which has only one nonzero value – being 1 – located on its j^{th} diagonal element. This double-focusing procedure is equivalent to depth migration. The double-focused result can be written as

$$\begin{aligned}\delta_j \mathbf{P}(z_m) = \mathbf{F}_w^{+}(z_m, z_d)\mathbf{D}^{-}(z_d)\mathbf{W}^{-}(z_d, z_m)\delta_j \mathbf{R}^{\cup}(z_m) \\ \mathbf{G}^{+}(z_m, z_s)\mathbf{S}^{+}(z_s)\mathbf{F}_w^{-}(z_s, z_m),\end{aligned} \tag{3}$$

where, $\mathbf{F}_w^{+}(z_m, z_d)$ and $\mathbf{F}_w^{-}(z_s, z_m)$ are the detector and source focusing matrices, which are the conjugates of primary-wave propagation matrices $\mathbf{W}^{-}(z_d, z_m)$ and $\mathbf{W}^{+}(z_m, z_s)$. Matrix $\delta_j \mathbf{R}^{\cup}(z_m)$ can be expressed as a vector-vector multiplication

$$\delta_j \mathbf{R}^{\cup}(z_m) = \mathbf{i}_j(z_m)\mathbf{i}_j^{\dagger}(z_m), \tag{4}$$

where, $\mathbf{i}_j(z_m)$ represents a unit column vector of which element j has a value of 1 while all other elements are 0, and the symbol $\dagger$ indicates a row vector.

Using this, equation (1) can then be simplified to

$$\delta_j \mathbf{P}(z_m) = \delta_j \mathbf{d}(z_m)\delta_j \mathbf{s}^{\dagger}(z_m), \tag{5}$$

Here, $\delta_j \mathbf{d}(z_m)$ and $\delta_j \mathbf{s}^{\dagger}(z_m)$ are the focal detector beam (a column vector) and focal source beam (a row vector), defined by

$$\delta_j \mathbf{d}(z_m) = \mathbf{F}_w^+(z_m, z_d)\mathbf{D}^-(z_d)\mathbf{w}_j(z_d, z_m)$$
$$\delta_j \mathbf{s}^\dagger(z_m) = \mathbf{g}_j^\dagger(z_m, z_s)\mathbf{S}^+(z_s)\mathbf{F}_w^-(z_s, z_m), \tag{6}$$

where $\boldsymbol{w}_j(z_d, z_m)$ and $\mathbf{g}_j^\dagger(z_m, z_s)$ are detector and source propagation vectors, with the superscripts "+" and "−" being removed for simplicity. According to the above definition of detector and source beams, the resolution vector $\delta_j \mathbf{p}(z_m)$, which is composed of the diagonal elements of the double-focused matrix $\delta_j \mathbf{P}(z_m)$, can be expressed as

$$\delta_j \mathbf{p}(z_m) = \delta_j \mathbf{d}(z_m) \cdot \delta_j \mathbf{s}^\dagger(z_m), \tag{7}$$

where the symbol $\cdot$ means the scalar (element-by-element) product. Note that in equation (3), multiples are included in the modeling operators but excluded in the focusing operators, which means all multiples are treated as noise in this way of carrying out migration (unless multiples are removed by some prestack multiple elimination process). Equation (3) can be used to estimate the focal source beam related to primaries in open-loop migration under the influence of multiples being considered as noise.

On the other hand, currently, multiples are no longer treated as noise in migration, but utilizing multiples in imaging has become a growing trend over the last few years (see e.g., Berkhout, 2012, 2014, 2016, 2018; Davydenko and Verschuur, 2016, 2018). After separating the wavefield into different-order parts, e.g. using the closed-loop SRME method (Lopez and Verschuur, 2015), the separated-order source-beam vectors can also be calculated with the independent open-loop migration such that:

$$\delta_j \mathbf{s}_w^\dagger(z_m) = \mathbf{w}^\dagger(z_m, z_s)\mathbf{S}^+(z_s)\mathbf{F}_w^-(z_s, z_m)$$
$$\delta_j \mathbf{s}_{m_1}^\dagger(z_m) = \mathbf{m}_1^\dagger(z_m, z_s)\mathbf{S}^+(z_s)\mathbf{F}_{m_1}^-(z_s, z_m) \tag{8}$$
$$\delta_j \mathbf{s}_{m_2}^\dagger(z_m) = \mathbf{m}_2^\dagger(z_m, z_s)\mathbf{S}^+(z_s)\mathbf{F}_{m_2}^-(z_s, z_m),$$

where $\mathbf{w}^{\dagger}(z_m)$, $\mathbf{m}_1^{\dagger}(z_m)$ and $\mathbf{m}_2^{\dagger}(z_m)$ are separated-order source propagation vectors (we dropped the subscript *j* for notational simplicity), $\mathbf{F}_{\bar{w}}^{-}(z_s, z_m)$, $\mathbf{F}_{\bar{m}_1}^{-}(z_s, z_m)$ and $\mathbf{F}_{\bar{m}_2}^{-}(z_s, z_m)$ are the corresponding focusing matrices that correspond to $\mathbf{w}^{\dagger}(z_m)$, $\mathbf{m}_1^{\dagger}(z_m)$ and $\mathbf{m}_2^{\dagger}(z_m)$. Substituting them into equation (7) yields the resolution function, which represents the ideal images of the fully order-separated wavefields. Their resolution is often higher than the actual resolution because the different-order wavefields cannot be separated exactly for field data under conditions of imperfect sampling of sources and detectors as well as the inaccurate migration velocities. Note that order-separated multiples usually contain wavefields with different travel paths. After applying open-loop focusing operators, only parts of the multiples can be focused well and the defocused parts can manifest as crosstalk noise.

To illustrate the open-loop focal beams based on one-step migration, we first give an example using the 3D layered velocity model shown in Figure 2a, with the target being set at (3, 3, 1) km. For full sampling of detectors and sources on the surface, the open-loop source beam results computed according to equation (8) are shown in Figures 4a-c, which represent source beams of the primaries, the first-order multiples, and the second-order multiples, respectively. If the primary-wave focusing operator is used, the primaries focus well (Figure 4a). If a multiple-wave focusing operator is used, the separated different-order multiples can also be imaged (Figures 4b-c). Comparisons show that the multiples provide a similar temporal resolution (Figure 4d) but a somewhat lower spatial resolution (Figure 4e) than primaries. This is because the multiples have smaller average incident angles than the primaries, which means a smaller spatial bandwidth. When the more complicated SEG/EAGE salt dome model (Figure 3a) is used, with the same parameters as in the previous example, the

resulting source beams (Figures 5e-d) show similar properties. In the beams of multiples shown in Figures 4b-c and Figures 5b-c, some crosstalk noise can be observed. This is because the multipath multiples cannot be focused and their defocused parts manifest as crosstalk noise. These examples indicate, in the framework of open-loop migration, that the use of multiples doesn't have benefits in the case of a full sampling of sources and detectors.

[Figure 4]

[Figure 5]

Closed-loop focal beams based on iterative inversion

As discussed in the previous section, the open-loop multiple-wave migration may suffer from crosstalk noise. Therefore, it is not surprising that multiples have typically been treated as noise that need to be removed before the application of open-loop migration. In this section, based on iterative inversion-based migration, we extend the full-wavefield focal beams (Kumar et al., 2015, 2016) to an order-controlled, closed-loop focal beam method, which provides the flexibility to analyze migration operators and resolution functions with the order-controlled surface and internal multiples.

Starting with the full-wavefield modeling defined in equation (1), we apply closed-loop double focusing at both detector and source sides of a unit angle-independent point diffractor $\delta_j \mathbf{R}^{\cup}(z_m) = \mathbf{i}_j(z_m)\mathbf{i}_j^{\dagger}(z_m)$ at a target point (x_j, y_j, z_m), followed by the imaging principle. The resulting closed-loop double-focused result can be written as

$$\delta_j \mathbf{P}_{g_n}(z_m) = \delta_j \mathbf{d}(z_m)\delta_j \mathbf{s}_{g_n}^{\dagger}(z_m). \tag{9}$$

Here, $\delta_j \mathbf{s}_{g_n}^{\dagger}(z_m)$ is the n^{th}-order closed-loop focal source beam, defined by

$$\delta_j \mathbf{s}_{g_n}^{\dagger}(z_m) = \mathbf{g}_j^{\dagger}(z_m, z_s)\mathbf{S}^{+}(z_s)\mathbf{F}_{g_n}^{-}(z_s, z_m), \tag{10}$$

where, $\mathbf{F}_{g_n}^{-}(z_s, z_m)$ is the n^{th}-order closed-loop source focusing operator related to the maximum order of multiples being $n-1$. In the double-focusing matrix $\delta_j \mathbf{P}_{g_n}(z_m)$, all the diagonal elements generate the resolution function $\delta_j \mathbf{p}_{g_n}(z_m)$, which can be calculated by an element-by-element multiplication of the focal-detector and the focal-source beams, as follows

$$\delta_j \mathbf{p}_{g_n}(z_m) = \delta_j \mathbf{d}(z_m) \cdot \delta_j \mathbf{s}_{g_n}^{\dagger}(z_m). \tag{11}$$

For the primaries-only case ($n = 1$), $\mathbf{F}_{g_1}^{-}(z_s, z_m)$ simplifies to the source focusing function of least-squares migration (Nemeth et al., 1990). For the multiple-included cases ($n \geq 2$), the full-wavefield propagator $\mathbf{G}_n$ is nonlinear and multiple-included, and the focusing matrix $\mathbf{F}_{g_n}^{-}$, being the inverse of $\mathbf{G}_n$, can no longer be approximated sufficiently well by the complex conjugate of $\mathbf{G}_n$. Instead, it can be estimated by solving a minimization problem with the following objective function

$$J = \sum_{\omega} \left\| \mathbf{i}_j^{\dagger}(z_m) - \mathbf{g}_{j,n}^{\dagger}(z_m, z_s)\mathbf{S}^{+}(z_s)\mathbf{F}_{g_n}^{-}(z_s, z_m) \right\|_2^2, \tag{12}$$

where, $\mathbf{g}_{j,n}^{\dagger}(z_m, z_s)$ is the n^{th}-order full-wavefield source propagation vector related to the $(n\text{-}1)^{\text{th}}$ order of multiples. Because of the limited temporal and spatial bandwidth of seismic data, the vector $\mathbf{i}_j^{\dagger}(z_m)$ should be replaced by the full-sampling primary-wave imaging vector $\hat{\mathbf{i}}_j^{\dagger}(z_m)$

$$J = \sum_{\omega} \left\| \hat{\mathbf{i}}_j^{\dagger}(z_m) - \mathbf{g}_{j,n}^{\dagger}(z_m, z_s)\mathbf{S}^{+}(z_s)\mathbf{F}_{g_n}^{-}(z_s, z_m) \right\|_2^2, \tag{13}$$

where,

$$\hat{\mathbf{i}}_j^{\dagger}(z_m) = \mathbf{w}_j^{\dagger}(z_m, z_s)\mathbf{F}_w^{-}(z_s, z_m). \tag{14}$$

The minimization problem above can be solved by an iterative gradient scheme to estimate the n-order focusing operator $\mathbf{F}_{g_n}^{-}$, followed by the calculation of the n-order focal source beam $\delta_j \mathbf{s}_{g_n}^{\dagger}$ using equation (10). Equation (13) can be performed in the frequency-space domain (e.g., Blacquiere et al., 1989; Wapenaar et al., 2014) or the frequency-wavenumber domain (e.g., Fu, 2006; Chen et al., 2017). Substituting equation (10) into equation (11) yields the closed-loop resolution function, which represents the image of the full-wavefield closed-loop migration.

To illustrate the closed-loop focal beams based on iterative inversion, we give an example using the 3D layered model shown in Figure 2a. The target is located at (3, 3, 1) km. The 3D acquisition geometry comprises a full sampling of detectors and sources on the surface. Figure 6 shows the resulting n-order closed-loop source focusing operators (left) and focal source beams (right) ($n = 1, 2, \text{and } 3$). Figure 6a shows the results of the first-order full-wavefield migration ($n = 1$), corresponding to least-squares migration, and Figures 6b-c show the results of the n^{th}-order full-wavefield migration ($n = 2 \text{ and } 3$). With the increasing order of n, the focusing operators (left) reach further in the positive time direction to remove more multiples, and the resulting focal source beams (right) provide a similar resolution but decreasing crosstalk noise. Moreover, the second-order closed-loop focal beam is enough to suppress most of multiples. In this case of $n = 3$, because of the simple-layered model and fully sampled geometry, the primaries achieve a full spatial illumination of the subsurface target, and all the multiples are removed by the focusing operators. Note that the multiple removal here has been done in the closed-loop migration process. No prestack multiple suppression is carried out before migration.

[Figure 6]

Examples

As discussed in the previous sections, when the primaries have been sampled perfectly, the multiples do not help to improve the spatial resolution and are automatically removed in the closed-loop migration. In practice, however, seismic acquisition geometries are always imperfect, e.g. with narrow apertures, large line intervals, or acquisition obstacle areas. A complex overburden may also weaken the illumination of the subsurface targets by primaries. Therefore, in practice, multiples could be treated as valuable supplements to primaries in the framework of the closed-loop migration, which will be discussed in several cases below.

1) Source sampling with a gap

In this example, we use again the 3D layered model shown in Figure 3a. The target locates at (3, 3, 1) km. The 3D acquisition geometry, shown in Figure 7, has a full detector sampling but has an incomplete source sampling with a 1 km gap along the *x* direction. Figure 8 shows the open-loop (a) and n^{th}-order closed-loop (b-d) source focusing operators (left) as well as the resulting focal source beams (right) ($n = 1, 2, \text{and } 3$). Because of the gap in the source sampling, all the focusing operators contain this gap as well, rather than being spatially continuous curves as Figure 6 shows. The focal beams are no longer the well-known cross shape but contain strong migration noise. As shown in Figures 8b-d, to fill in the gap of primary-wave illumination for the target, the closed-loop focusing operators contain energy at times smaller than the time of the primary focusing operator (shown in Figure 8a). This

energy images some parts of multiples. This energy was not used in the previous example, where the source sampling was perfect. Note that the energy contained at times larger than the time of the primary focusing operator will have a multiple-suppression effect, while energy contained at times smaller than the time of the primary focusing operator will have a multiple-usage effect. The higher-order closed-loop focusing operators contain energy both at larger and smaller times than the time of the primary focusing operator to deal with higher-order multiples correctly, i.e., both suppress and use higher-order multiples, depending on whether the primary illumination can take proper care of the imaging or not. As a result, the closed-loop focal beams (Figures 8b-d) provide a similar spatial resolution but lower migration noise than the open-loop focal beams (Figure 8a). As shown in the rectangular areas of Figure 8, the higher the multiple order the less the migration noise. Note that, however, migration noise cannot be eliminated and the effects of acquisition geometries need to be evaluated.

[Figure 7]

[Figure 8]

2) Layered model with a high-velocity block

Figure 9 shows a 3D layered model with a high-velocity block. We place the target at (3, 3, 1) km and use two acquisition geometries that have different source apertures of 2 km (left) and 6 km (right) along both x and y directions. Figure 10 shows the resulting open-loop (a) and n^{th}-order closed-loop focal source beams (b-d) ($n = 1, 2, \text{and } 3$). Compared with those

shown in Figure 8, with the gap in the source sampling, the high-velocity overburden decreases the spatial bandwidth of the migration image and produces more serious migration noise because of multiple reflections and scattering at the upper and lower boundaries of the block. The closed-loop migration can suppress more noise than the open-loop migration, and the larger the multiple-wave order involved the better the noise suppression. On the other hand, by enlarging the acquisition apertures from 2 km (left) to 4 km (right), the resulting focal beams achieve better noise suppression, especially in the area near the target. This example illuminates the importance of choosing the proper acquisition apertures and the use of a high-order closed-loop migration algorithm for imaging the targets below the complicated overburden.

[Figure 9]

[Figure 10]

3) Complex 3D SEG/EAGE salt dome model

We apply our method to a cropped version of the 3D SEG/EAGE salt dome model shown in Figure 3a. The acquisition geometry has a 1 km gap in its source sampling along the x direction shown in Figure 7. The combination of the complex model and the sampling gap are expected to produce the resulting beams with more complicated noise patterns. As in the modeling case, we set the target position at (3, 3, 1) km just beneath the salt dome. For the full acquisition geometries, we calculate the open-loop and n^{th}-order closed-loop source focusing operators as well as the focal source beams ($n = 1, 2, \text{and } 3$). As shown in Figure 11,

the complex SEG/EAGE salt dome model complicates the propagation of seismic wavefields, which leads to complex results for both open-loop and closed-loop focal beams. In Figure 11a, the open-loop focusing operator (left) is no longer a simple single-event curve as in the simple-layered media, and the open-loop focal beam (right) no longer equals the well-known X shape. In Figures 11b-d, with the increasing order n, the closed-loop focusing operators have more energy in both the positive and the negative time directions, which means that more multiples are used to improve the spatial resolution, while also more multiples are removed to minimize the crosstalk noise. The high-order closed-loop focal operators almost reach the upper and lower limits of the timeline to utilize and remove as many multiples as possible in the migration. Thus, Figure12 shows the closed-loop focal beams provide higher spatial resolution and less migration noise than the open-loop focal beams. The comparison of different-order closed-loop beams show that high-order closed-loop beams may show similar resolution but slightly less migration noise.

[Figure 11]

[Figure 12]

4) Impact of inaccurate migration velocities

We use the 3D layered velocity model shown in Figure 2a to illustrate the effect of an inaccurate velocity model on the spatial resolution. We set the target at (3, 3, 1) km and use two acquisition geometries: one with full source sampling and the other one with an incomplete source sampling, i.e. with a 1 km gap along the x direction (Figure 7). Different

from all the previous examples, to compute our focussing operators (**F**) we now use inaccurate velocities with a relative error of 20% with respect to the correct velocities used in the modeling part (**W**). This approach is considered to be representative for the case the the velocities are often not known precisely in advance. Figure 13 shows the resulting open-loop (a) and n^{th}-order closed-loop focal source beams (b-d) ($n = 1, 2, \text{and } 3$) of the full acquisition geometry (left) and the gapped geometry (right). The inaccurate migration velocities lead to phase shifts of both primaries and multiples. All wavefields cannot be focused well at the target location at zero time and manifest as migration noise. As shown in the left panel of Figure 13, when the primaries have been sampled perfectly, multiples are not involved in imaging and they can be removed completely even with the wrong migration velocities. However, in the right panel of Figure 13, when the primaries are not sampled well, some parts of the multiples are involved in imaging and cannot not be removed well with the wrong migration velocities, especially for the high-order closed-loop migration. This is because the high-order multiples travel the longest propagation distances and are most susceptible to the velocity error. The high-order closed-loop migration needs a more accurate velocity model than the low-order closed-loop migration and the open-loop migration. At the same time, this means that is the high-order closed-loop forward modeling could be used in velocity analysis or inversion to provide a more accurate velocity model than lower-order modeling.

Discussion

We compare the temporal and spatial resolution of primary and multiple reflections in open-loop focal beams in different media. Results show, when multiples are involved, that the

open-loop migration neither avoids crosstalk noise, nor uses simultaneously primaries and multiples to achieve a higher resolution. Therefore, it is not surprising that multiples have traditionally been treated as noise that needs to be removed before the application of open-loop migration.

We then extend the focal beam theory to the order-controlled closed-loop focal beam method, which provides the flexibility to analyze migration operators and resolution functions with full control over the order of surface and internal multiples in the process of iterative inversion-based migration. Based on the results of source focusing operators and focal source beams, we investigate the effects of multiple wavefields on the imaging quality for different acquisition geometries and different overburden strata, such as a narrow observation aperture, an acquisition obstacle area, a high-velocity overburden, and a complex salt dome. Closed-loop migration results show that the question of whether multiples should be considered to be signal or noise depends on whether the primaries provide full spatial illumination of the subsurface target. When the answer is yes, e.g., for a simple, layered overburden and a proper-sampled acquisition geometry, the closed-loop migration removes all multiples. However, when the answer is no, e.g., for a complex overburden or a limited-aperture acquisition geometry, the closed-loop migration can use some multiples that provide independent illumination to fill in the gap of primary-wave sampling, while at the same time can remove some multiples to reduce the related noise. Whether multiples are used or suppressed can be recognized by the structure of the focusing operators: events at earlier times than the times of the primary focusing operator correspond to using multiples in the imaging, while events at later times correspond to suppressing multiples.

The order-controlled closed-loop focal beam analysis provides varying degrees of efficiency depending on the maximum order of multiples involved in migration, as its implementation becomes more time-consuming with increasing order of multiples. Thus, it is important to choose the optimal maximum order of multiples to improve the efficiency of the closed-loop focal beam analysis. Our examples show that the multiple-wave order can be chosen according to the main purpose of the acquisition analysis. If we aim to analyze the effects of acquisition geometries on the multiple-wave suppression, the second-order closed-loop focal beam is recommended. However, if we aim to analyze the effects of acquisition geometries on achieving high-resolution imaging by strengthening the azimuthal illumination of shadow zones, a higher-order closed-loop focal beam should be used. Similarly, our analysis also provides suggestions on how to choose the optimal maximum order of multiples in the closed-loop migration, in which we can choose the second-order closed-loop migration for suppressing most of the strongest multiples, or a higher-order closed-loop migration for achieving the best resolution.

We also discuss the effect of inaccurate migration velocity on the spatial resolution. Results show the high-order closed-loop migration is more susceptible to the velocity errors than the low-order closed-loop migration and the open-loop migration. It needs a more accurate velocity model than the traditional migrations. On the other hand, this means that the high-order closed-loop migration is also expected to be useful in velocity inversion to provide a more accurate velocity model than the traditional migration methods.

Note that we only consider the focal source beams and do not consider the effects of the imaging conditions (e.g. deconvolution) and prestack denoising on multiple-wave suppression.

Although our analysis here is not completely fair to the migration approaches irrelevant to multiples, e.g., least-squares migration, our results above are still valid in that multiples cannot be fully removed in practice, especially considering internal multiples. Our analysis can also be improved further by considering more physical factors, such as ghost waves, surface waves, converted waves, and elastic waves.

Conclusions

We introduce an order-controlled closed-loop focal beam method, with application to the resolution analysis of seismic acquisition geometries. It provides the flexibility to analyze migration operators and resolution functions with full control over the order of surface and internal multiples taken into account in the process of iterative inversion-based migration. This method can be used in seismic acquisition geometry design with multiples being considered as either noise or signal. With this method, we investigate the effects of different-order wavefields on the imaging quality for different acquisition geometries and different overlying strata structures, e.g. narrow observation apertures, acquisition obstacle areas, high-velocity blocks and more complicated salt structures. Results show, in the acquisition geometry design, when the primaries cannot provide a complete spatial illumination of the subsurface target, e.g., because of a limited aperture or a complex overburden, we should use the closed-loop focal beam analysis to assess the complicated effects of multiples considered as both signal and noise. The multiple-wave order should be chosen according to the main purpose of the acquisition analysis. We can choose the second-order closed-loop focal beam to analyze the effects of acquisition geometries on multiple suppression, and we can choose a higher-order closed-loop focal beam to analyze the

effects of acquisition geometries on high-resolution migration. Finally, this method can also be used to choose the optimal order of multiples to take into account in closed-loop migration.

Data availability statement

The data that support the findings of this study are available from the corresponding author upon request.

References

Berkhout, A. J., 1982, Seismic migration, imaging of acoustic energy by wave field extrapolation: A—Theoretical aspects: Elsevier Science.

Berkhout, A. J., 1997, Pushing the limits of seismic imaging, Part I: Prestack migration in terms of double dynamic focusing: Geophysics, 62, 937–953.

Berkhout, A.J., 2012, Combining full wavefield migration and full waveform inversion: a glance into the future of seismic imaging: Geophysics, 77(2), S43–S50.

Berkhout, A. J., 2014, Review paper: An outlook on the future of seismic imaging. Part II: Full-wavefield migration: Geophysical Prospecting, 62, 931–949.

Berkhout, A. J., 2016, Utilization of multiple scattering: the next big step forward in seismic imaging. Geophysical Prospecting, 1–40.

Berkhout, A. J., 2018, Closed-loop multiple-scattering imaging with sparse seismic measurements. Geophysical Journal International, 212, 1766–1790.

Berkhout, A. J., L. OngKiehong, A. W. F. Volker, and G. Blacquiere, 2001, Comprehensive assessment of seismic acquisition geometry by focal beams—Part I: Theoretical considerations. Geophysics, 66(3), 911–917.

Beylkin, G., 1985, Imaging of discontinuities in the inverse scattering problem by inversion of a causal

generalized Radon transform: Journal of Mathematical Physics, 26, 99–108.

Blacquiere, G., H. W. J. Debeye, C. P. A. Wapenaar, and A. J. Berkhout, 1989, 3-D tabledriven migration: Geophysical Prospecting, 37, 925–958.

Cao, J. and R. S. Wu, 2009, Full-wave directional illumination analysis in the frequency domain: Geophysics, 74(4), S85–S93.

Chen, G., L. Y. Fu, W. Wei, and W. Sun, 2017, Wavefield interpolation in 3D large-step Fourier wavefield extrapolation: Geophysical Prospecting, 1–16.

Cordsen, A, M. Galbraith, and J. Peirce, 2000, Planning land 3-D seismic surveys: SEG.

Davydenko, M., and D. Verschuur, 2017, Full-wavefield migration: Using surface and internal multiples in imaging: Geophysical Prospecting, 65, 7–21.

Davydenko, M., and D. Verschuur, 2017, Including and using internal multiples in closed-loop imaging — Field data example: Geophysics, 83, R297–R305.

De Bruin, C. G. M., C. P. A. Wapenaar, and A. J. Berkhout, 1990, Angledependent reflectivity by means of prestack migration: Geophysics, 55, 1223–1234.

Fu L.Y., 2006, Comparison of different one-way propagators for wave forward propagation in heterogeneous crustal wave guides: Bulletin of the Seismological Society of America, 96, 1091–1113.

Lopez, G. A. and D. J. Verschuur, 2015, Closed-loop surface-related multiple elimination and its application to simultaneous data reconstruction: Geophysics, 80(6), V189–V199.

Gibson, R. L., and C. Tzimeas, 2002, Quantitative measures of image resolution for seismic survey design: Geophysics, 67, 1844–1852.

Huang, Y., G. T. Schuster, 2014, Resolution limits for wave equation imaging: Journal of Applied

Geophysics, 107, 137–148.

Ishiyama, T., G. Blacquière and W. A. Mulder, 2016, The impact of surface-wave attenuation on 3-D seismic survey design: Geophysical Prospecting, 1–11.

Jurick, D., J. Codd, F. Hoxha, J. Naumenko and D. Kessler, 2003, Gulf of Suez acquisition design using 2D and 3D full-wave equation simulation: 73rd Annual International Meeting, SEG, Expanded Abstracts, 2136–2139.

Kumar, A., G. Blacquière, and D. J. Verschuur, 2015, Extending illumination using all multiples: Application to 3D acquisition geometry analysis: Geophysical Prospecting, 1–20.

Kumar, A., G. Blacquière, M. W. Pedersen, and A. Goertz, 2016, Full-wavefield marine survey design using all multiples: Geophysics, 81(3), P15–P26.

Liu, Y. K., X. Chang, D. G. Jin, R. Q. He, H. C. Sun, and Y.C. Zheng, 2011, Reverse time migration of multiples for subsalt imaging: Geophysics, 76(5), Wb209–Wb216.

Lu, Shaoping, D. N. Whitmore, A. A. Valenciano, and N. Chemingui, 2015, Separated-wavefield imaging using primary and multiple energy: The Leading Edge, 34(7), 770–772, 774–776, 778–778.

Nemeth, T., C. Wu, and G. T. Schuster, 1999, Least-squares migration of incomplete reflection data: Geophysics, 64, 208–221.

Regone, C. J., 2006, A modeling approach to wide-azimuth design for subsalt imaging: The Leading Edge, 25(12), 1467–1475.

Schuster, G. T., G. Dutta, J. Li, 2017, Resolution limits of migration and linearized waveform inversion images in a lossy medium, Geophysical Journal International, 209(3), 1612–1621.

Thorbecke, J. W., C. P. A. Wapenaar, and G. Swinnen, 2004, Design of oneway wavefield extrapolation operators, using smooth functions in WLSQ optimization: Geophysics, 69, 1037–1045.

Tu, N., and F. J. Herrmann, 2015, Fast imaging with surface-related multiples by sparse inversion: Geophysical Journal International, 201, 304–317.

Van Veldhuizen, E. J., G. Blacquière, and A. J. Berkhout, 2008, Acquisition geometry analysis in complex 3D media: Geophysics, 73, Q43–Q58.

Vermeer, G. J. O., 1999, Factors affecting spatial resolution: Geophysics, 64(3), 942–953.

Vermeer, G. J. O., 2012, 3-D seismic survey design: SEG.

Verschuur, D.J. and A. J. Berkhout, 1994, Multiple technology, part 1: estimation of multiple reflections: Annual International Meeting, SEG, Expanded Abstracts, 1493–1496.

Volker, A. W. F., G. Blacquière, A. J. Berkhout, and L. OngKiehong, 2001, Comprehensive assessment of seismic acquisition geometry by focal beams—Part II: Practical aspects and examples: Geophysics, 66, 918–931.

Wapenaar, C. P. A., 1998, Short note – Reciprocity properties of oneway propagators: Geophysics 63(5), 1795–1798.

Wapenaar, K., J. Thorbecke, J. van der Neut, F. Broggini, E. Slob, and R. Snieder, 2014, Marchenko imaging: Geophysics, 79(3), WA39–WA57.

Wei, W., L. Y. Fu and G. Blacquière, 2012, Fast multifrequency focal beam analysis for 3D seismic acquisition geometry: Geophysics, 77(2), P11–P21.

Wei, W., and L. Y. Fu, 2014, On horizontal resolution for seismic acquisition geometries in complex 3D media: Journal of Applied Geophysics, 108, 43–52.

Wu, R. S., and L. Chen, 2006, Directional illumination analysis using beamlet decomposition and propagation: Geophysics, 71, S147–S159.

Xie, X. B., S. Jin, and R. S. Wu, 2006, Wave-equation-based seismic illumination analysis: Geophysics,

71, S169–S177.

Yan, Z. and X. B. Xie, 2016, Full-wave seismic illumination and resolution analyses: A Poynting-vector-based method: Geophysics, 81(6), S447–S458.

List of Figures

Figure 1: Grid-point response for primary and multiple reflections.

Figure 2: (a) The 3D layered velocity model with the source marked by a star, (b) the direct wavefield (1st iteration), (c) first-order multiple wavefield (2nd iteration) and (d) second-order multiple wavefield (3rd iteration) produced by the FWMod. The seismic amplitudes are displayed with a 90% clip, which is used in all following figures.

Figure 3: (a) The cropped 3D SEG/EAGE salt dome velocity model with the source marked by a star, (b) the direct wavefield (1st iteration), (c) first-order multiple wavefield (2nd iteration), and (d) second-order multiple wavefield (3rd iteration) produced by the FWMod.

Figure 4: Open-loop Focal beams in a 3D layered model for (a) the direct wavefield, (b) first-order multiple wavefield and (c) second-order multiple wavefield and the slices along the t- (d) and x- (e) directions.

Figure 5: Open-loop Focal beams in a 3D SEG/EAGE salt dome model for (a) the direct wavefield, (b) first-order multiple wavefield and (c) second-order multiple wavefield and the slices along the t- (d) and x- (e) directions.

Figure 6: Closed-loop source focusing operators (left) and focal beams (right) in a 3D layered model related to the maximum order of multiples being 0 (a), 1 (b) and 2 (c).

Figure 7: The 3D layered velocity model is shown with the gapped source sampling marked

by the brick shading. The stars indicate to the target location.

Figure 8: Open-loop (a) and closed-loop focal operators (left) and beams (right) in a 3D layered model with the maximum order of multiples being 0 (b), 1 (c) and 2 (d). The dashed rectangles mark the difference of migration noise among beams.

Figure 9: The 3D layered model with a high-velocity block with the narrow (left) and wide (right) source sampling marked by the brick shadows. The stars represent the target locations.

Figure 10: Open-loop and closed-loop focal source beams in the 3D block model (Figure 9) related the maximum order of multiples being 0 (b), 1 (c) and 2 (d), in which the left and right panels correspond to different source sampling lengths of 2 km and 4 km.

Figure 11: Open-loop and closed-loop source focusing operators (left) and focal beams (right) of the gapped acquisition geometry (Figure 7) in the cropped 3D SEG/EAGE salt dome model (Figure 3) related to the maximum order of multiples being 0 (b), 1 (c) and 2 (d).

Figure 12: Target-crossing vertical (left) and horizontal (right) profiles for the open-loop and closed-loop focal beams (Figure 11).

1

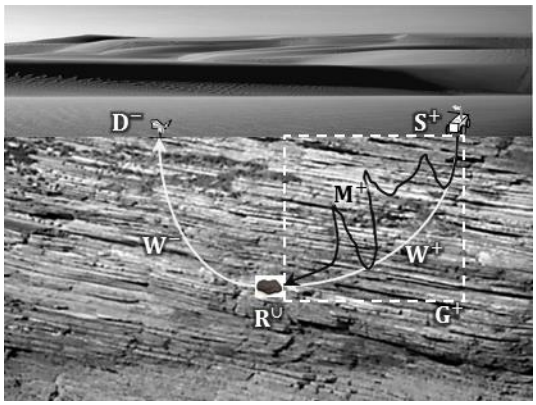

2 **Figure 1**: Grid-point response for primary and multiple reflections

3

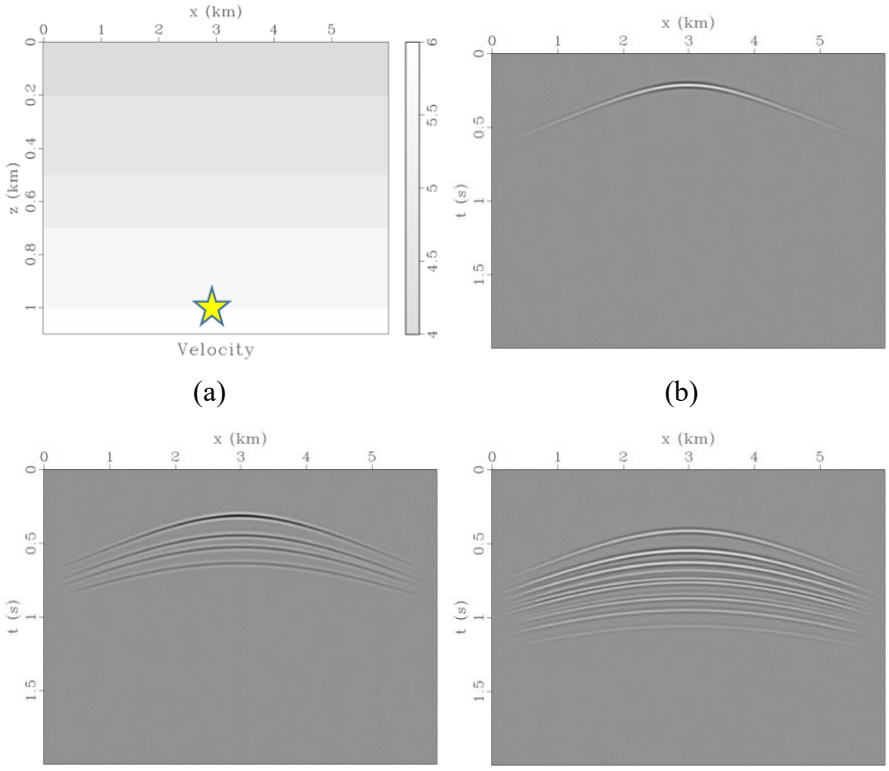

Figure 2: (a) The 3D layered velocity model with the source marked by a star, (b) the direct wavefield (1st iteration), (c) first-order multiple wavefield (2nd iteration) and (d) second-order multiple wavefield (3rd iteration) produced by the FWMod. The seismic amplitudes are displayed with a 95% clip, which is used in all following figures.

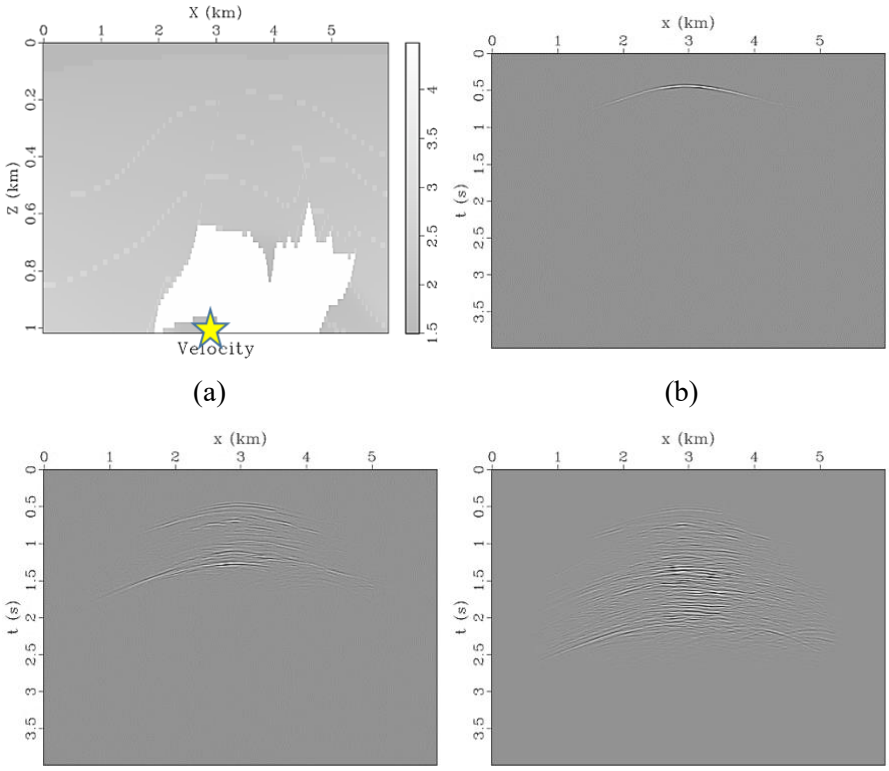

Figure 3: (a) The cropped 3D SEG/EAGE salt dome velocity model with the source marked by a star, (b) the direct wavefield (1st iteration), (c) first-order multiple wavefield (2nd iteration), and (d) second-order multiple wavefield (3rd iteration) produced by the FWMod.

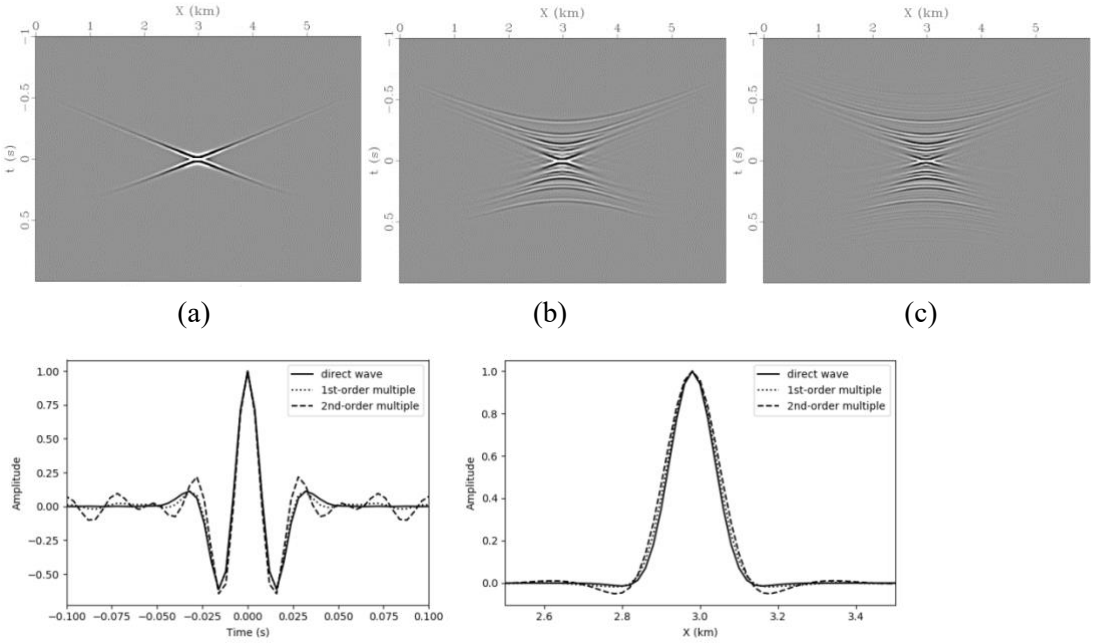

Figure 4: Open-loop Focal beams in a 3D layered model for (a) the direct wavefield, (b) first-order multiple wavefield and (c) second-order multiple wavefield and the slices along the t- (d) and x- (e) directions.

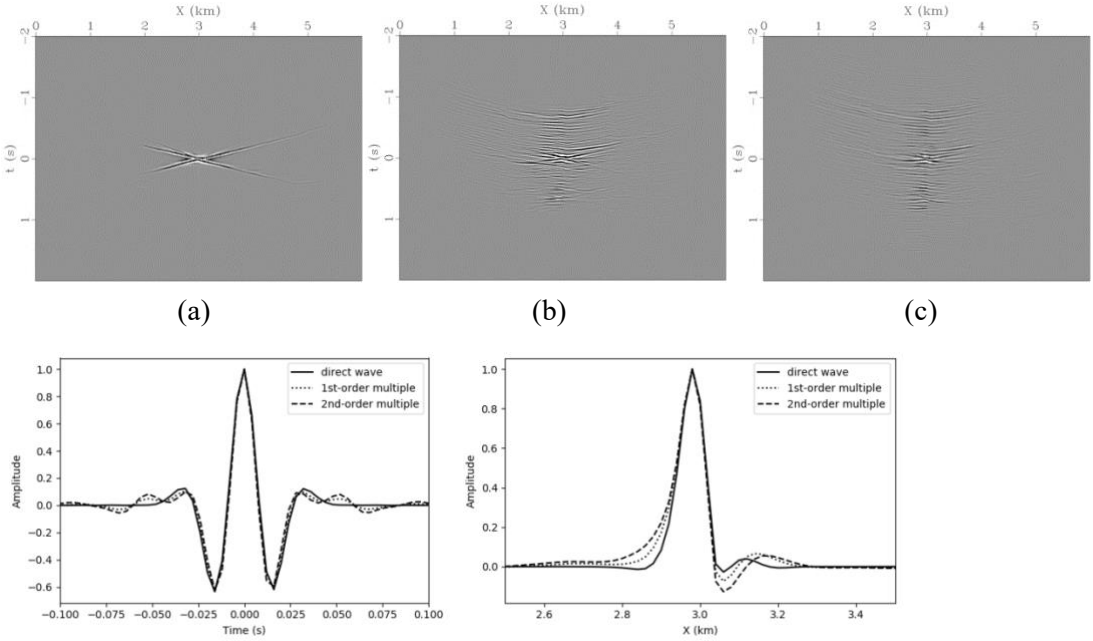

Figure 5: Open-loop Focal beams in a 3D SEG/EAGE salt dome model for (a) the direct wavefield, (b) first-order multiple wavefield and (c) second-order multiple wavefield and the slices along the t- (d) and x- (e) directions.

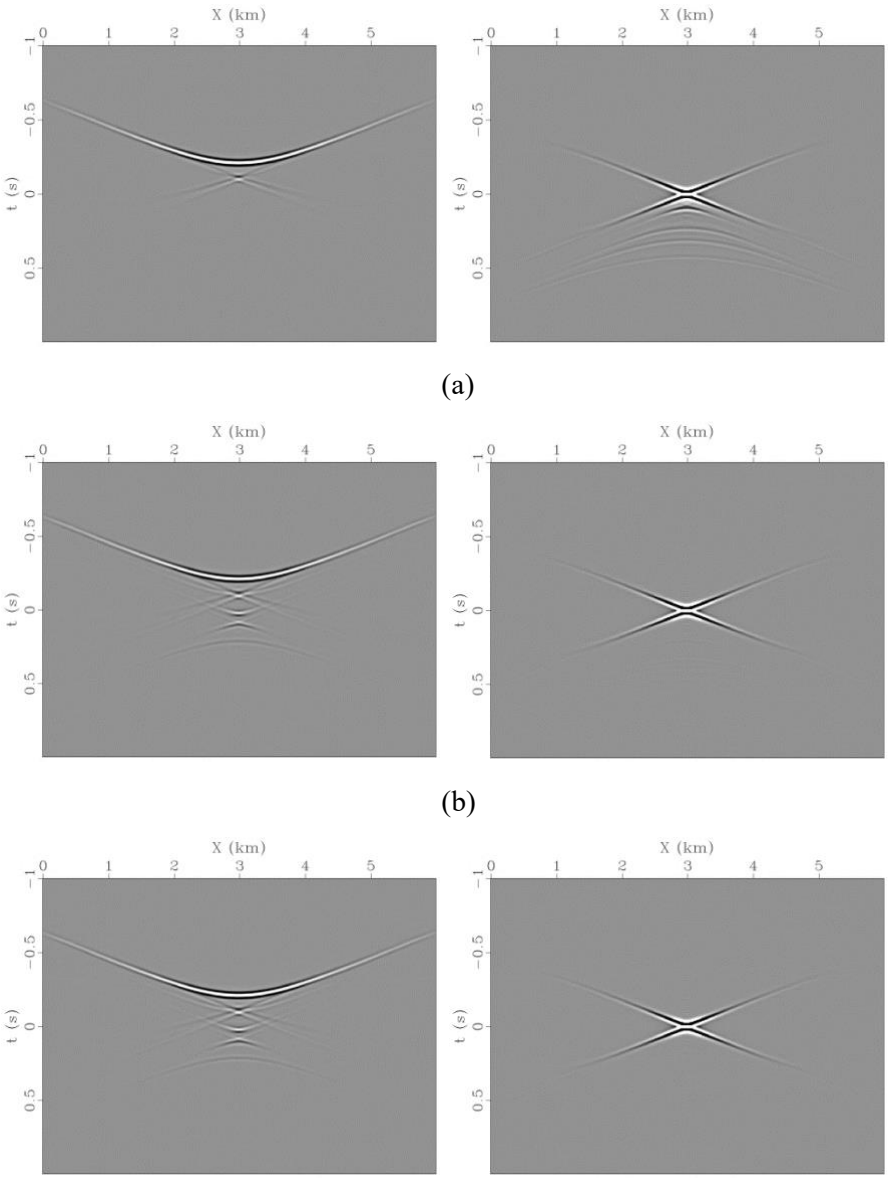

Figure 6: Closed-loop source focusing operators (left) and focal beams (right) in a 3D layered model related to the maximum order of multiples being 0 (a), 1 (b) and 2 (c).

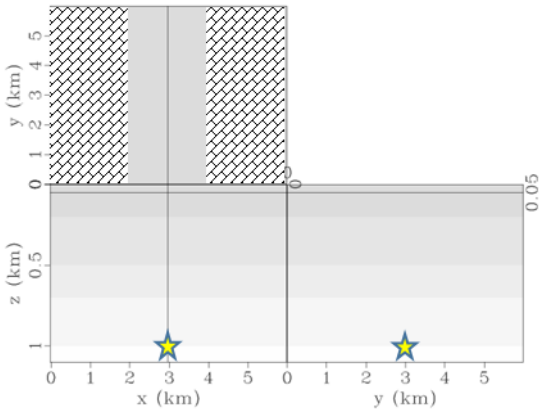

Figure 7: The 3D layered velocity model is shown with the gapped source sampling marked by the brick shading. The stars indicate to the target location.

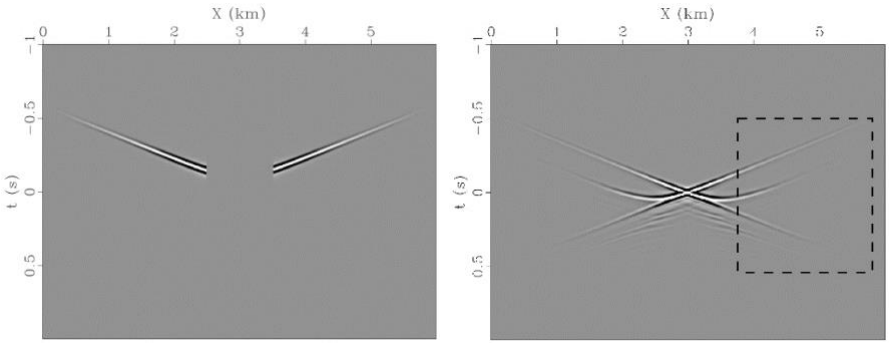

(a)

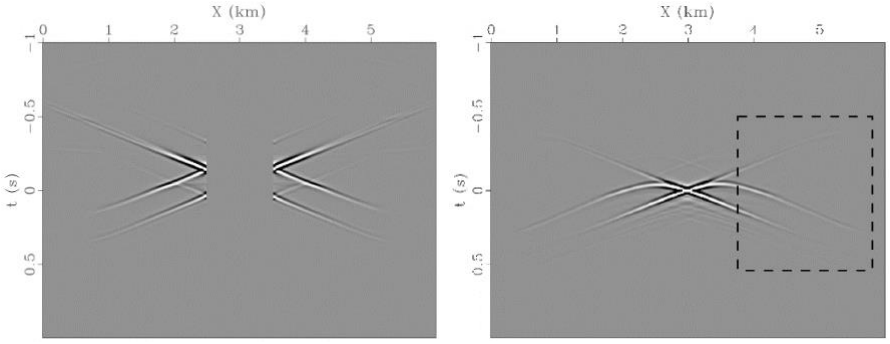

(b)

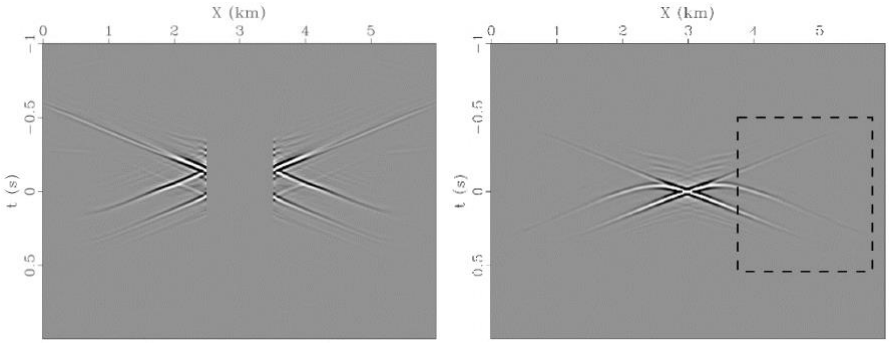

(c)

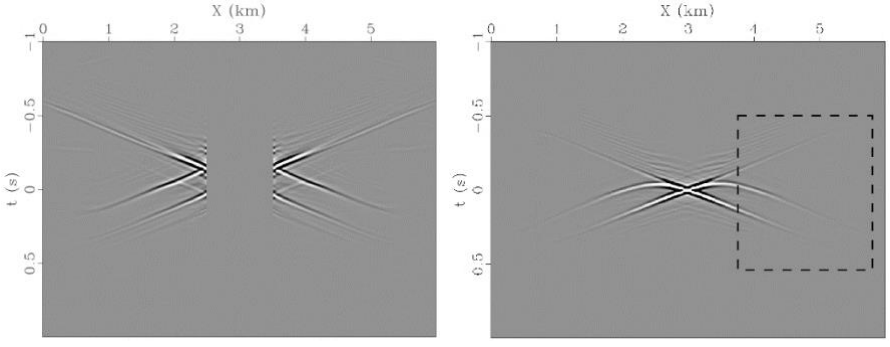

(d)

Figure 8: Open-loop (a) and closed-loop focal operators (left) and beams (right) in a 3D layered model with the maximum order of multiples being 0 (b), 1 (c) and 2 (d). The dashed rectangles mark the difference of migration noise among beams.

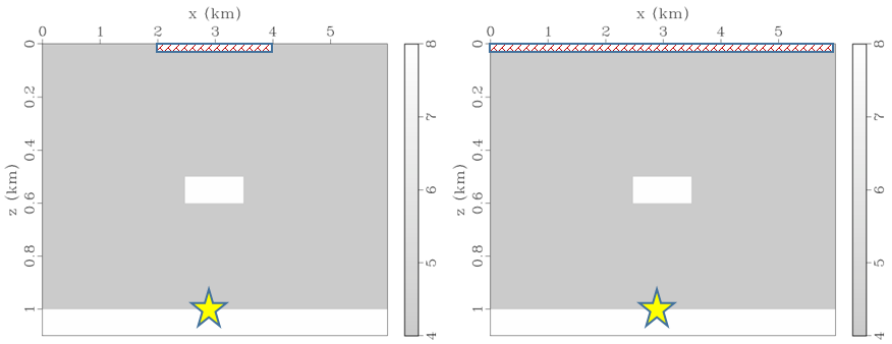

Figure 9: The 3D layered model with a high-velocity block with the narrow (left) and wide (right) source sampling marked by the brick shadows. The stars represent the target locations.

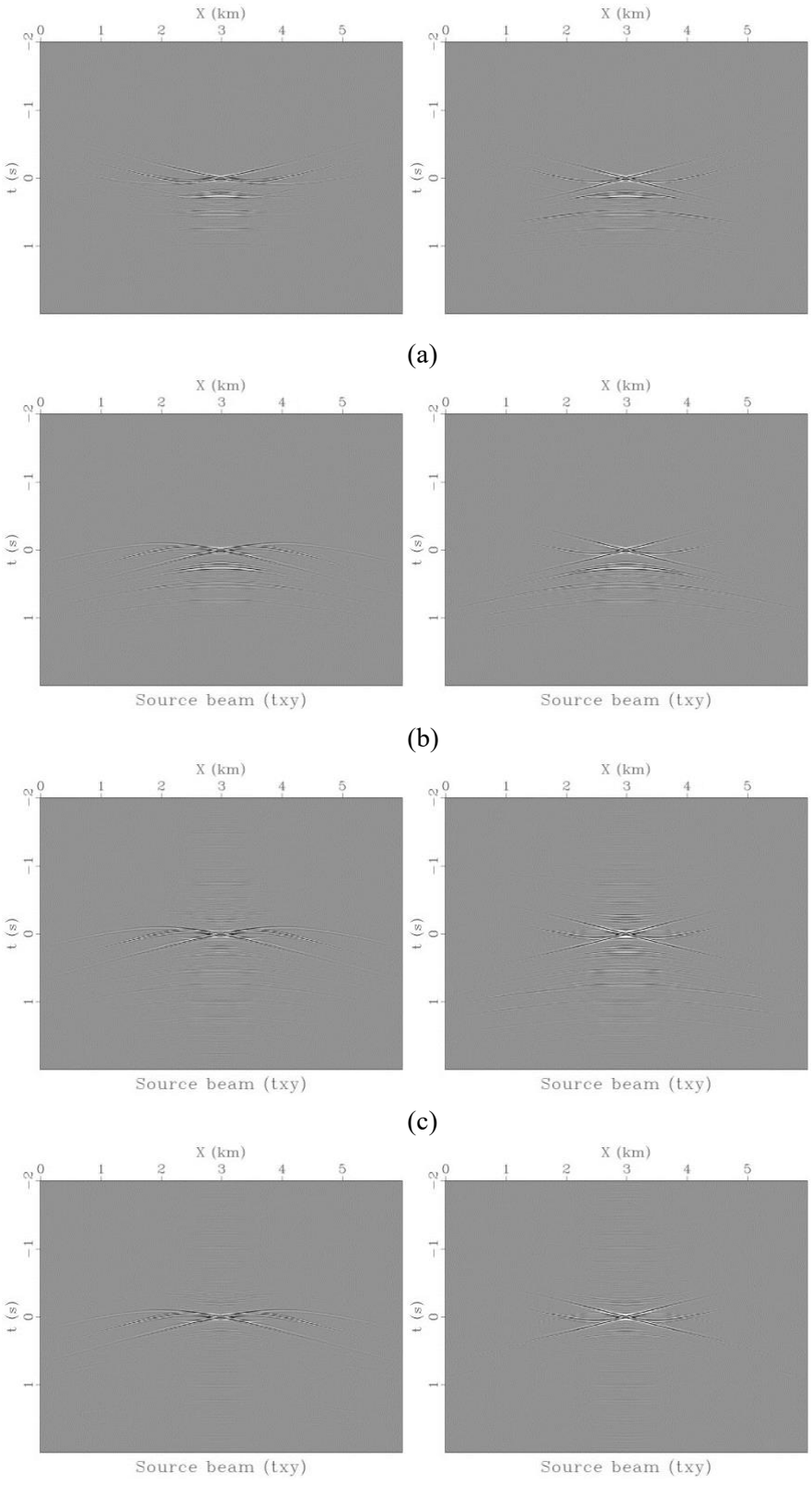

Figure 10: Open-loop and closed-loop focal source beams in the 3D block model (Figure 9) related the maximum order of multiples being 0 (b), 1 (c) and 2 (d), in which the left and right panels correspond to different source sampling lengths of 2 km and 4 km.

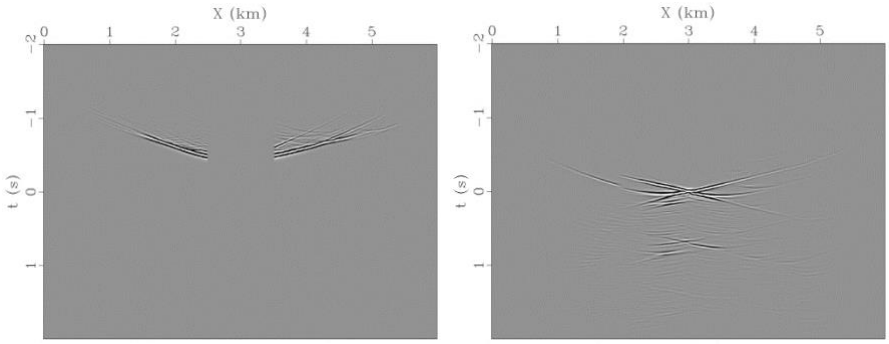

(a)

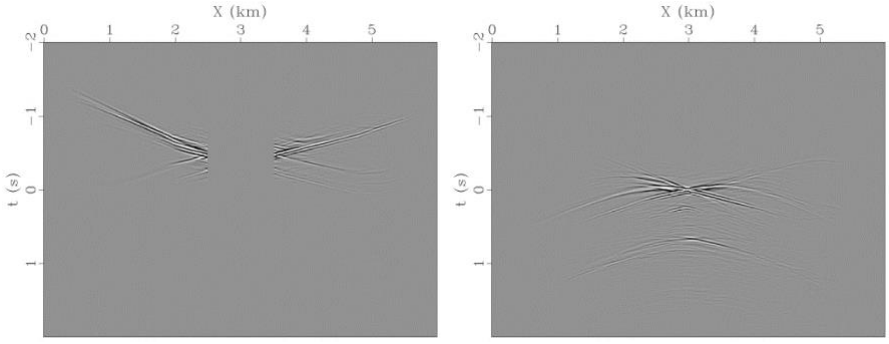

(b)

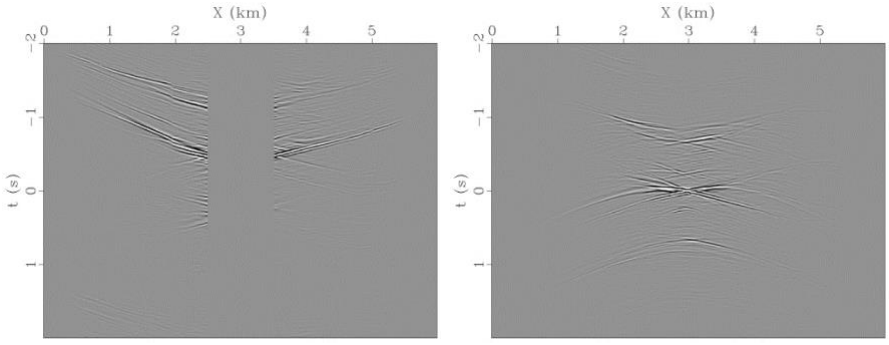

(c)

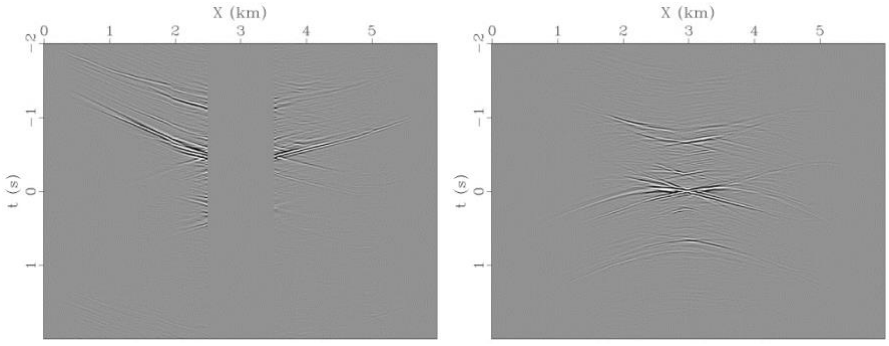

(d)

Figure 11: Open-loop and closed-loop source focusing operators (left) and focal beams (right) of the gapped acquisition geometry (Figure 7) in the cropped 3D SEG/EAGE salt dome model (Figure 3) related to the maximum order of multiples being 0 (b), 1 (c) and 2 (d).

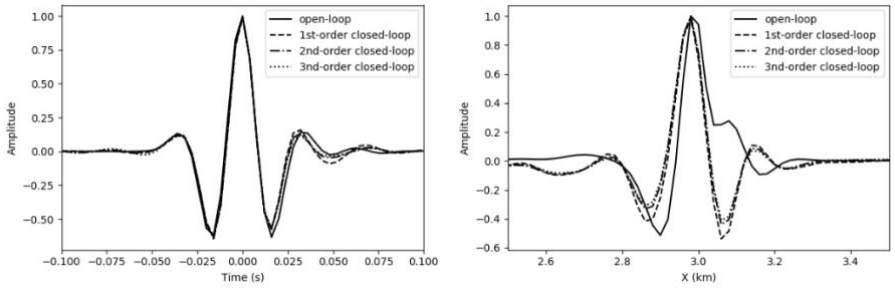

Figure 12: Target-crossing vertical (left) and horizontal (right) profiles for the open-loop and 1st, 2nd, and 3rd-order closed-loop focal beams (Figure 11) related to the maximum order of multiples being 0, 1 and 2.

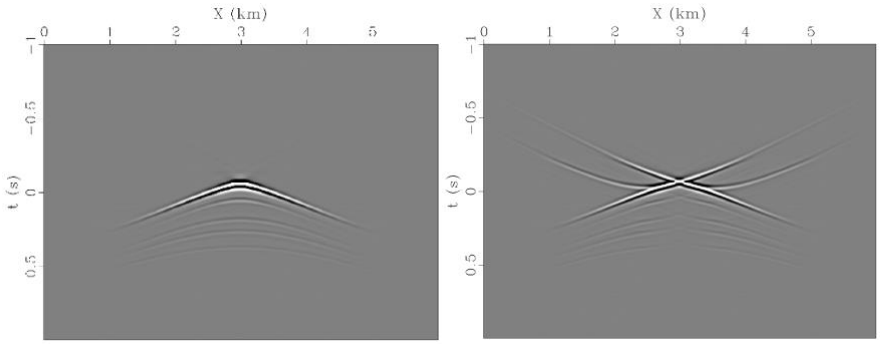

(a)

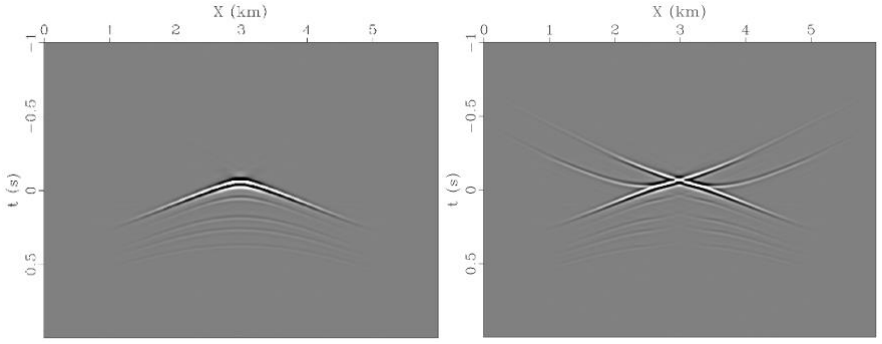

(b)

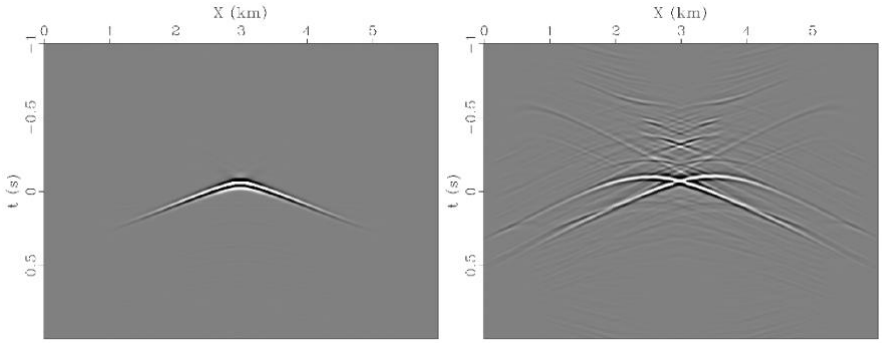

(c)

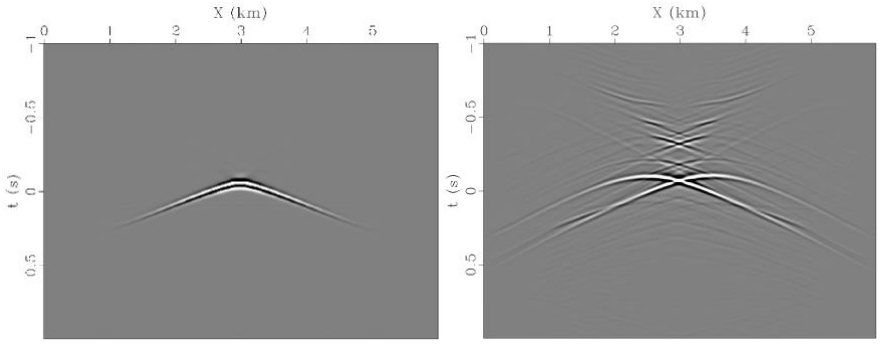

(d)

Figure 13: Open-loop (a) and closed-loop focal beams model with the maximum order of multiples being 0 (b), 1 (c) and 2 (d) resulting from the inaccurate migration velocities, which have a relative error of 20% with respect to the modeling velocities. The left panel shows the results of a full acquisition geometry, and the right panel showsj the results of an incomplete

1 acquisition geometry with a 1 km gap along the x direction (Figure 7).
2